Egypt. J. Microbiol. **59,** pp. 75-94 (2024)

EgyptianJournalofMicrobiology
http://ejm.journals.ekb.eg/

One-Step Green Facile Fabrication of Chitosan Nanoparticles, Characterization and Application Against Building-Colonizing Meristematic Fungi

Hadeel El-Shall[1*], Noura El-Ahmady El-Naggar[2], Asmaa A. El-Sawah[3], Marwa Eltarahony[1*]

[1]Environmental biotechnology department, Genetic engineering and biotechnology research institute (GEBRI), City of scientific research and technological applications (SRTA-City), New Borg El-Arab City 21934, Alexandria, Egypt.

[2]Department of Bioprocess Development, Genetic Engineering and Biotechnology Research Institute, City of Scientific Research and Technological Applications (SRTA-City), New Borg El-Arab City 21934, Alexandria, Egypt.

[3]Medical Microbiology and Immunology Department, Faculty of Medicine, Mansoura University, Mansoura, Egypt.

BIO-deterioration of buildings is a significant challenging issue worldwide. Therefore, the current study quested for finding ecofriendly approach against building bio-deteriorator microbes. Chitosan nanoparticles (CNPs) are natural polymeric nanoparticles with unique characteristics and exhibits potent antimicrobial activities, making them a promising eco-friendly material for biocontrol. Thus, this study describes an alternative, green synthesis approach for CNPs using the cell free supernatant of *Paradendryphiella* sp. as a crosslinking and stabilizing agent. The SEM and TEM analyses showed that CNPs are spherical particles, with sizes ranging from 10.1 to 26.08 nm. The presence of several bands in the FTIR spectrum shows the existence of capping agents that stabilize CNPs. X-ray diffraction reveals the crystalline structure of CNPs. A time-dependent antifungal assay of CNPs was implemented against *Exophiala dermatitidis* as a model of slow growing meristematic black fungi that causes building biodeterioration. The results revealed that upon employing the higher doses of CNPs (250 and 500 µg/mL), significant fungicidal potency was exhibited within 33 and 57 h exposure time, with significant (*P*–value < 0.0001) lethality rate (K-value) of -0.06 and -0.009 CFU/ml/h, respectively. Further, SEM micrographs illustrated the prevalence of morphologically deteriorated macroconidia or budding yeast cells without polymeric matrix of biofilm with minor presence of crinkled mycelia and avoiding of pseudo-hyphae and sclerotic bodies, reflecting thereby the losing of cells pathogenicity through lethal antimycotic potentiality of CNPs. Hence, the current study highlights the possibility of employing the mycogenically fabricated CNPs as hygienic coating in maintaining building structures from bioreceptivity and biodeterioration.

Keywords: Chitosan nanoparticles; *Paradendryphiella* sp.; green synthesis; characterization; *Exophiala dermatitidis*; antifungal activity; building biodeterioration.

Introduction

In the recent epoch, The settlement of atmospheric water vapor that contained sulfurous, nitrogenous and carbonaceous aerosols, which stems from fossil fuels, traffic discharge, urbanization, industrial/ domestic wastes and agricultural effluents, onto buildings worsened markedly the problem of building corrosion/ deterioration. Remarkably, the presence of outdoor or airborne microorganisms simultaneously with all previous combination would accelerate biocorrosion/ biodeterioration of buildings and disrupt the quality of

*Corresponding Author's information Hadeel El-Shall E-mail: hadeel.elshall28@gmail.com & helshall@srtacity.sci.eg
Marwa Eltarahony E-mail: m_eltarahony@yahoo.com & meltarahony@srtacity.sci.eg

Received 7/11/2024 ; Accepted 11/11/2024
DOI: 10.21608/EJM.2024.334410.1265

©2024. National Information and Documentation Center (NIDOC)

cultural/historical heritage. Such detrimental process could be implemented through sequential steps, begins with microbial colonization of the building materials via various strategies such as superficial penetration (i.e., epilithic), intra distances invasion between fissures and crevices (i.e., chasmolithic) and deep penetration to some millimeters or centimeters (i.e., endolithic), as reported by Scheerer et al. (2009). The phototrophic colonizing microbes (e.g., cyanobacteria, algae and lichens) assimilate CO_2 by utilizing stone materials as nutrient source, followed by the generation of metabolic byproducts that consumed by other heterotrophic colonizers of bacteria and fungi, which also multiply in a continuous metabolic process; followed by yielding progressively different metabolites of pigments, enzymes, inorganic acids (e.g., sulfuric acid, nitric acid, nitrous acid and sulfurous acid) and organic acids (e.g., citric, oxalic, malic, succinic, fumaric, formic, gluconic, glyoxylic, acetic and tartaric acids). Interestingly, such heterotrophic colonizers possess the ability to be developed in biofilm lifestyle, in which the individual communities consolidate their assembly in a potent extracellular polymeric matrix (EPS). Through biofilm structure, the biodeteriorator microbes could withstand harsh atmospheric conditions and invade tightly and deeply wider areas in either vertical and/or horizontal expansions (Liu et al. 2020). Generally, it is plausible to mention that biocorrosion is caused by the synergistic interaction of different microbial genera rather than solitary work.

Subsequently, the accumulation of these metabolic byproducts would induce unfavorable alterations in buildings both aesthetically and structurally. Actually, their interaction with stone materials ingredients and forming a complex with metal cations and clay matrices would result in chemical alterations, physical deformations, destabilizing the mineral lattices, discolouration, decaying painting/glues, destroying the internal/external stone structure and utterly cracking of building stone material, as reported by "Encyclopedia of Bioprocess Technology" (Banach et al. 2014). Strikingly, all these microbial deteriorating symptoms were frequently observed in numerous buildings such as bridges, silos, dams, maritime structures, hospitals, food processing/storage constructions and even in historic buildings (e.g., Giza pyramid and Seti I Tomb in Egypt and La Palma in Spain) (Liu et al. 2020).

Noteworthy stating that the filamentous fungi, in particular meristematic/black fungi, unequivocally and aggressively symbolize an intrinsic contribution in building biodeterioration phenomenon. The major symptom of such corrosion is black crusts and biopitting, particularly in tropic and Mediterranean regions, which formed through extending their hyphae superficially and penetrating them deeply in stone fissures with enlarging the stone porosity (Berti et al. 2023). Broadly, saprophytic basidiomycetes such as *Trichosporon asahii* and ascomycetes like *Exophiala*, *Penicillium*, *Alternaria*, *Aspergillus*, *Sarcinomyces Trimmatostroma* and *Chaetomium* are the most popular biodeteriogens that dwell divergent ecological niches including mural paintings (Pinna, 2021; Joseph, 2021; Subramanian et al. 2022). Meanwhile, such fungal biodeteriogens could also threaten human health, causing serious health problems such as allergic diseases, organ mycoses and mycotoxicosis, especially in immunosuppressed individuals, through their bio-aerosols that include mycotoxins, volatile metabolites and pigments (Gutarowska et al. 2012; Ganguli et al. 2021). Therefore, it is necessary to comply laws and legislations in employing eco-labelling hygienic coatings in building structures to lessen bioreceptivity and reduce the rate of biodeterioration, in a safe way for people and pets' health. Accordingly, the amalgamation of polymer manufacturing and nanotechnology deemed as a promising solution (Aldosari et al. 2019).

Currently, chitosan nanoparticles (CNPs) were widely applied in conquering microbes by the dint of their natural polymeric origin in nanostructure scales. However, their colorless nature facilitates their applications as painting constituent in construction industry, hence, fulfilling the aesthetic requirements, which was missing object in many inorganic biocides (Sierra-Fernández *et a*l. 2017).

Chitosan nanoparticles (chitosan-NPs) have been produced using many chemical and physical techniques, such as the ionic gelation method (Nasti *et al*. 2009), supercritical-CO_2-assisted solubilization, emulsification and crosslinking, ionic gelation with radical polymerization self-assembly, and precipitation-based techniques, atomization and spray drying. Numerous drawbacks of chemical and physical processes include the application of high pressure, hazardous chemicals, high temperatures, big generated particles, etc. (Yanat and Schroën, 2021). In previous literature, Van *et al*. (2013) stated that the nano spray drier produced CNPs between 300 and 3500 nm, with an average size of 1000 nm depending on spray cap hole size. Using tripolyphosphate (TPP) ionic gelation in combination with spray drying, Nguyen *et al*. (2017) found that the mean size of CNPs generated ranged from 166 to 1230 nm, depending on the diameter of the spray dryer needles and the molecular weight of chitosan. According to the findings of Ha *et al*. (2019), the TPP and chitosan solution ionic gelation method was used to create CNPs, and the resulting

size distribution varied between 300 and 750 nm. A range of 277–731 nm was used for generating self-assembled chitosan nanoparticles (Mukhopadhyay *et al*. 2013). Bekmukhametova *et al*. (2022) concluded that developing a protocol for the synthesis of CNPs with a diameter of 200–300 nm is still challenged.

The fields of biomedical engineering, pharmaceuticals, and nanomedicine have prospective applications for CNPs, which have a size range of 10 to 80 nm (Sharifi-Rad *et al*., 2021). Therefore, it is imperative to establish environmentally secure methods for the bio-fabrication of ultrafine CNPs with a size of less than 100 nm, since these particles are needed for a variety of applications (El-Naggar *et al*. 2024). Ultrafine chitosan-NPs were produced by an environmentally friendly processes (Sathiyabama and Parthasarathy, 2016; El-Naggar *et al*. 2022a; El-Naggar *et al*. 2022b, El-Naggar *et al*. 2022c; El-Naggar *et al*. 2023a; El-Naggar *et al*. 2023b).

Materials and Methods

Microorganism and culture maintenance

The fungus *Paradendryphiella sp.* was isolated, identified previously and submitted in GenBank under accession number of OQ134928 (El-shall *et al*. 2023). *Exophiala dermatitidis* strain was purchased from Moubasher Mycology Center at University of Assiut, Egypt. The Czapek-Dox medium was used to culture *Paradendryphiella* sp., which included the following ingredients (g/L): 30 sucrose, 3 sodium nitrate, 0.5 potassium chloride, 0.5 magnesium sulfate heptahydrate, 1 di-potassium hydrogen phosphate, 0.01 iron (II) sulfate heptahydrate. While, sabouraud dextrose agar (SDA) with ingredients (g/L) (40 dextrose and 10 peptone) was used to culture *E. dermatitidis* the pH of both media was set to a value of 5.5 and 15 Agar. The incubation process continued for a period of five days at a temperature of 30 ºC. The plates were subsequently stored at a temperature of 4 ºC for future use.

CNPs biosynthesis

A piece of low molecular weight chitosan (Poly-(1,4-b-D-glucopyranosamine) was purchased from Bio Basic Inc. (Markham, Ontario L3R 8T4 Canada). It had the following characteristics: a viscosity ranging from 60 to 300, a deacetylation degree of ≥90%, and a molecular weight of 20 KDa. Chitosan was dissolved at a concentration of 1% w/v in 1% acetic acid and subjected to magnetic agitation for a duration of 24 hours. 1N NaOH was then utilized to bring the pH to 5. In a 250-mL Erlenmeyer flask supplemented with fifty mL of Czapek-Dox broth medium, the fungal strain was cultivated for 5 days at 30ºC. Following the incubation period, the mycelia of the fungal strain were separated through centrifugation at 5000×g for duration of 15 minutes. To produce CNPs, the resulting cell-free supernatant was utilized in accordance with the methodology outlined by El-Naggar *et al*. (2023a). At room temperature, an equivalent volume of chitosan solution was mixed with the cell-free supernatant (2 mL). The produced turbidity was centrifuged at 10000×g for 10 minutes and washed. For further characterization, the produced turbidity was freeze-dried.

UV-Visible spectrum

Using an Optizen Pop-UV-visible spectrophotometer, the biosynthesized CNPs were analyzed to confirm the formation of nanoparticles and to ascertain the maximal absorbance wavelength. The wavelength range at which the CNPs solution was scanned in the range of 200–800 nm.

Fourier transform infrared spectroscopy (FTIR)

FTIR was used to determine the functional groups that are present in both CNPs and the capping agents surrounded the CNPs by measuring the quantity of infrared light an object absorbs over a variety of wavelengths. The CNPs sample was crushed using KBr pellets for surface properties analysis. The FTIR spectra in the range of 4000–500 cm^{-1} were measured at a resolution of 1 cm^{-1} using the Shimadzu FTIR-8400S spectrophotometer.

X-ray diffraction analysis

The X-ray diffractometer (Bruker D2 Phaser 2nd Gen) was employed to detect the crystalline nature and mean size of the dried powder CNPs. The X-ray diffractometer operated at 30 kV and a current of 15 mA with Cu Kα radiation (λ = 1.506 Å) and a scanning rate of 5 min^{-1}. The 2θ scanning range was six degrees to sixty degrees. The X-rays that are generated are focused and are directed toward a sample of CNPs. A diffracted beam is generated by the interaction between the sample and incoming rays, and it is subsequently detected, processed, and recorded. A diffraction pattern is demonstrated by plotting the intensity of the diffracted rays that are scattered at different angles of the CNPs (Raja *et al*. 2022).

Microscopy analysis of CNPs

The size, shape, and degree of crystallinity of CNPs were investigated using TEM "JEM-2100 Plus, JEOL Ltd., Japan". Through the use of a focused, high-energy electron beam, a TEM may transmit the specimen and produce an image that can be seen on a phosphor screen, or imaging system, located on the other side of the electron beam that is impinging. TEM specimen was prepared by the simple deposition

of a dilute suspension of the CNPs on a carbon-coated copper grid. The surface shape and size of CNPs can be directly observed via SEM. SEM uses a concentrated, high-energy electron beam to image the surface of CNPs through a tiny layer of metal or carbon that must be sputter-coated on CNPs. The elemental composition information of the CNPs specimen was detected using EDX (the same apparatus of SEM).

ζ-potential of the biosynthesized CNPs

ζ-potential is an important technique that can reveal the net surface charge of the CNPs by detecting the electrostatic attraction or repulsion between particles and is also considered a reliable predictor of the stability of the CNPs solution. ζ potential can be used to precisely determine the behavior of the suspended colloids or nanoparticles (El-Naggar *et al*. 2022a). The surface charge and ζ potential of CNPs were measured using a Malvern 3000 Zetasizer (Nano ZS, UK) with a laser Doppler and detected using phase analysis light scattering (El-Naggar *et al*. 2023a). CNPs sample was diluted with deionized water with a viscosity of 0.887 cP to avoid numerous scattering effects (Çakır et al. 2020). Prior to analysis, a high-speed homogenizer was used to homogenize the diluted CNPs sample for 10 minutes at 13,000 rpm. It was subsequently immersed in an ultrasonic bath. After the sample had been dispersed, the nanoparticles were counted at a rate of 348.9 kcps (kilo counts per second) for 60 seconds using 5.5 mm of calibrated space at a temperature of 25ºC (El-Naggar et al. 2023b). The hydrodynamic diameter averages for multiple CNPs were calculated to get mean values.

Thermogravimetric analysis (TGA) and Differential scanning calorimetry (DSC) of CNPs

The thermal stability of the CNPs was investigated by measuring the glass transition (T_g) and melting temperature (T_m). To learn more about the CNPs' thermal stability, DSC and TGA tests were carried out. Once the CNPs sample dried out for an hour at 60ºC, it was transferred onto a platinum sample pan. The sample was exposed to temperatures ranging from ambient temperature to 800ºC. TGA was conducted on a 3.81 mg sample of CNPs using a thermos-analyzer model 50-H in a nitrogen atmosphere at a flow rate of 10 mL min^{-1} and a temperature raised by 10ºC/ minute. The percentage of weight loss was plotted versus the temperature (El-Naggar et al. 2023a). Thermal denaturation of the CNPs sample was estimated using DSC. The sample was subjected to temperatures that varied from ambient to 800ºC. In a nitrogen atmosphere, a sample of CNPs (1.81 m g) was subjected to DSC analysis at a flow rate of 30 mL $min^{-1}$and a heating temperature of 10 °C min^{-1}.

Time-kill assay

The strain of *Exophiala dermatitidis*, as a representative model for building deterioration meristematic fungi, was purchased from Moubasher Mycology Center, Assiut University (AUMMC), Egypt. In order to define the effect of different concentration of CNPs with different time intervals during the incubation period in the fungal death process, such technique was employed via macro dilution broth method based on the Clinical and Laboratory Standard Institute CLSI guideline. In brief, 100 µL of *Exophiala dermatitidis* suspensions (5 x 10^5 CFU/) was poured into tubes containing Sabouraud dextrose broth (2 mL) with different doses of CNPs (50, 125, 250, 500 and 1000 µg/mL). In addition, a control tube of fungal suspension devoid from any treatment was run in parallel. All treated and control tubes were incubated at 30◦C and 150 rpm for 120h. Thereafter, aliquots were drawn from each culture at different time intervals (i.e., every 3 h.), cultured onto Sabouraud dextrose agar plates and incubated as previously described. The number of total living cells (CFU/mL) in each tube at every time intervals were calculated. Ultimately, the logarithm of counted live colonies was plotted versus time to construct the time-kill diagram, for declaring growth rate changes over time (Kim *et al*. 2020; Kim *et al*. 2022). Experiments were conducted in triplicates and Graphpad Instat software was used to statistically analyze the results and determine the significant differences (p-value ≤0.05). To define the change, either reduction or increase, in the fungal populations comparing to initial inoculums, the log 10 reduction and percentage decrease for each time point were calculated according to the following equations (Eq. 1 &2) (Ngene *et al*. 2024).

% Reduction = Initial count – Count at x time interval/ Initial count X 100 (Eq. 1)

Log10 reduction = Log10 (initial count) – Log10 (× time interval) (Eq. 2)

Mathematical model for fungicidal activity

The killing kinetics of the fungicidal activity were analyzed by fitting the mean data at each time point to an exponential equation: $N_t = N_0 \times e^{-Kt}$, where N_t expresses the number of viable yeasts at time t, N_0 is the number of viable fungal cells at the beginning of the experiment, K represents the killing (or lethality) rate, and t is the contact time. The exponential equation was transformed into a line by applying natural logarithms ($\log N_t = \log N_0 - Kt$). The goodness of fit of the data was calculated from the correlation coefficient (R^2; ranging from 0.8 to 0.98). The fungicidal activities were compared by use of the K values. Wherein, positive K value points out to the growth and the negative

values represents the killing (Cantón et al. 2004). Additionally, the discrimination between the fungicidal and fungistatic activity was identified as a decline of ≥3 log10 CFU/ mL from initial inoculum and no change comparing to the initial inoculum, respectively (Binesh *et al*. 2021; Khare *et al*. 2021).

Ultrastructure study of E. dermatitidis upon CNPs treatment

The morphological changes of fungus under study upon utilizing sub-lethal concentration of CNPs were examined via scanning electron microscope (SEM). The treated and untreated samples were prefixed in 2.5 % glutaraldehyde for 24 h at 4°C and dehydrated with gradient ethyl alcohol series (30:100%) for 15 min. The dried samples were subjected to a Polaron SC7620 Sputter Coater for gold coating step and inspected using SEM (JEOL JSM 6360LA, Japan) (El-Naggar et al. 2023a).

Results and Discussion

The biological approach used to synthesize CNPs from a variety of biological species, including plants, fungi, and actinomycetes is very efficient, inexpensive, safe, clean, and easy to use. In the present study, CNPs was biosynthesized extracellularly using the cell-free supernatant of *Paradendryphiella* sp. which is grown in a suitable medium. The broth containing fungal cells was centrifuged, and the supernatant containing fungal proteins is then used for the biosynthesis of CNPs. The supernatant containing proteins is allowed to crosslink with chitosan molecules. Anionic molecules in the cell-free supernatant of *Paradendryphiella* sp. diffuse into the positively charged chitosan molecules and crosslinking occurs results in the formation of CNPs. When positively-charged chitosan molecules are mixed with anionic molecules, crosslinking takes place and nanoparticles are formed (Yanat and Schroën, 2021). Chitosan nanoparticles synthesis is aided by the addition of acidic polysaccharides to chitosan solution; CNPs formation may be the result of simple electrostatic interaction (Sathiyabama et al. 2024).

Chitosan nanoparticles are capable of providing significant antimicrobial properties through various mechanisms. These include the interaction between positively charged chitosan nanoparticles and negatively charged plasma membrane phospholipids, the metal chelating potency of chitosan nanoparticles, and cell wall penetration capability, as well as DNA inhibition and the consequent hindering of mRNA synthesis (Xing *et al*. 2021).

UV-Vis absorbance of CNPs

After adding the cell-free supernatant of *Paradendryphiella* sp. to the chitosan solution, the first optical observation of CNPs biosynthesis is a suspended turbidity in the mixture, as shown in Figure 1A. The highest absorbance wavelength of the biosynthesized CNPs was determined by doing a wavelength range scan of 200 to 800 nm using a UV/Vis spectral scan (Figure 1B). The highest absorbance wavelength of CNPs was shown at 286 nm. The UV-visible spectrum of CNPs in the range of 200 and 322 nm is due to the presence of the C=O group (Duraisamy et al. 2022; El-Naggar *et al*. 2023a). Our result is consistent with the results of El-Naggar *et al*. (2023a) who utilized the *Lavendula angustifolia* leaf extract for the biosynthesis of CNPs with the highest absorbance wavelength of 285 nm, and Sathiyabama and Parthasarathy (2016) studies, who utilized proteins produced from *Penicillium oxalicum* for the biosynthesis of CNPs with the highest absorbance wavelength of 285 nm. The highest absorbance wavelength of CNPs biosynthesized by an aqueous extract of *Cympopogon citratus* leaves was detected at 295 nm (El-Naggar *et al*. 2024). Also, the CNPs that were produced from the leaf aqueous extract of *Pelargonium graveolens* showed the highest absorbance wavelength of 295 nm (El-Naggar *et al*. 2022a).

Microscopy analysis of CNPs

The analysis of the shape of biosynthesized CNPs using TEM and SEM is shown in Figure 2A & 2B, respectively, SEM shows nanoparticles in two dimensions or as a two-dimensional projection. The electrons interact with the CNPs to produce a variety of signals that reveal details about their composition and surface topography. All of the nanoparticles had a spherical in shape that was rather uniform, with a fairly constant particle size distribution according to the scanning electron micrographs. The TEM analysis of biosynthesized CNPs using the cell-free supernatant of *Paradendryphiella* sp. showed spherical particles with sizes ranging from 10.1 to 26.08 nm with mean of 18.63 ± 4.17 (Figure 2C). Comparing this study to the previous physical and chemical preparation of CNPs, our results have the smallest particle sizes. According to Wardani & Sudjarwo (2018), the SEM micrograph of CNPs revealed a rough surface morphology and spheres with sizes of around 500 nm. The SEM image of CNPs produced by the ball milling methodology has a rough surface and an irregular shape with a size of 247.3 ± 38.1 µm (Wardani et al. 2022). The typical particle sizes of the synthesized CNPs range from 33.64 to 74.87 nm in FE-SEM analysis. The size of the CNPs synthesized by the ionic gelation method with TTP and acetic acid showed a minimum size of 28.3 nm and a maximum of 46 nm in SEM (Raj et al. 2015).

Using the ionic gelation process, the positively charged chitosan and the negatively charged hydroxypropyl methylcellulose phthalate were combined to create CNPs, which were found to be stable and homogeneous in the 200–250 nm size range (Makhlof et al. 2011). According to Khanmohammadi et al. (2015), the diameter of CNPs produced by spray drying ranged from 700 to 3500 nm, with a mean size of 970 nm (Van et al. 2013). They also showed an average size of 420 nm across the 300–1500 nm range and an average size of 750 nm between 500–2500 nm. CNPs were synthesized by sodium tripolyphosphate (TTP), ranging in size from 100 to 400 nm (Zhang et al. 2010). The range of the CNPs size synthesized by natural di- and tricarboxylic acids was 60–280 nm observed by TEM, according to Bodnar et al. (2005).

By using the flow chemistry reactor and batch synthesis methods, they yielded CNPs with a spherical shape in TEM analysis, with the average size of the CNPs made by batch synthesis ranging from 30 to 120 nm and ~40–60 nm diameter made with the unique design flow chemistry reactor (Huanbutta et al. 2023). The main components and chemical composition of biosynthesized CNPs were examined using energy-dispersive X-ray spectroscopy (EDX) analysis. The EDX analysis of CNPs produced by the sell-free supernatant of *Paradendryphiella* sp. is displayed in Figure 2D. The obtained CNPs comprise carbon (95.05 %) and oxygen (3.95 %), according to EDX analysis. Nitrogen produces a very weak response making it difficult to detect for the biosynthesized CNPs sample.

Fourier transform infrared spectroscopy of CNPs

The FTIR analysis reveals the intermolecular interactions and identifies the functional groups that are present in the dried sample of CNPs and the capping agents that from the cell-free supernatant of *Paradendryphiella* sp. surrounded the nanoparticles. The FTIR spectrum (Figure 3A) showed ten absorption peaks (3943.6, 3437.26, 2934.79, 2142.99, 1630.87, 1389.76, 1306.82, 1082.1, 760.94, and 558.41cm^{-1}) of the obtained CNPs. The FTIR spectrum (Figure 3B) showed ten absorption peaks (3917.56, 3431.48, 2884.64, 2356.13, 2142.02 1651.12, 1603.86, 1383.97, 1324.18, 1083.07, and 585.42 cm^{-1}) of the chitosan standard. Figure 3C represented the FTIR of the cell-free supernatant of *Paradendryphiella* sp.. The first peaks (3943.6 and 3917.56 cm^{-1}) in the spectra of CNPs and chitosan, respectively, indicate that the combination of the functional groups of −NH_2, −CH, C−C, and −OH, emerged between 4057 and 3750 cm^{-1} (El-Naggar et al. 2023a). The peaks (3437.26 and 3431.48 cm^{-1}) of CNPs and chitosan, respectively indicate the presence of NH stretching that exists in -NH_2 in amides, aromatic amines, and primary amines. Notable variations in peaks locations between the CNPs and chitosan standard spectra suggest a significant involvement for functional groups presented in the cell-free supernatant of *Paradendryphiella* sp. in the biosynthesis of CNPs.

The peaks of 2934.79 cm^{-1} and 2884.64 in CNPs and chitosan, respectively are located between the range (2990–2850), which attributes to CH anti-symmetric and symmetric stretch that are present in −CH_3 and −CH_2− in alkanes (El-Naggar *et al*. 2023a; El-Sawah *et al*. 2024a). The peak at 2142.99 of CNPs spectrum indicates the presence of a C≡N stretch, which presents in thiocyanates. The peak at 1630.87 cm^{-1} reveals the existence of two bands from C=O stretch and NH_2 deformation founded in amide I in CNPs spectrum (Haris & Severcan, 1999; El-Sawah *et al*. 2024b). The peak at 1389.76 cm^{-1} in CNPs indicates the presence of O=C=O symmetric stretch that exists in COO^- group in carboxylic acid salts. The peak at 1306.82 cm^{-1} in CNPs represents the SO_2 anti-symmetric stretch presented in sulfones and also indicates the N=N−O symmetric stretch presented in azoxy compounds (Lambert, 1987). The peak at 1082.1 attributes the C−O stretch present in alcohols in CNPs (El-Sawah *et al*. 2024b). The peak at 760.94 cm^{-1} in CNPs attributes CH (out of plane deformation) presents in both monosubstitued and disubstituted benzenes. The peaks of 558.41 and 585.42 cm^{-1} in the spectra of CNPs and chitosan, respectively, attribute to NO_2 deformation bond, which presents in nitro compounds (Lambert, 1987). Only one peak (760.94 cm^{-1}) is due to the cell-free supernatant of *Paradendryphiella* sp.. The FTIR spectrum's small peaks at the end demonstrate the wiggling of the saccharide structure of chitosan (El-Naggar *et al.* 2022a; Rasaee et al. 2016). The presence of several strong bands in the FTIR spectrum indicates the presence of capping agents, which act as a stabilizer to prevent the CNPs overgrowth and stop their aggregation and/or coagulation in colloidal synthesis (El-Naggar et al. 2022a).

Zeta potential of CNPs

The biosynthesized CNPs was examined by Zeta potential, which is crucial by providing details on the charge of the CNPs as well as the tendency to remain distinct or aggregate inside a solution. The highly negative or positive zeta potential values cause higher repulsive forces, whereas repulsion between the nanoparticles with similar electric charge enhances stability, inhibits aggregation of the nanoparticles, and therefore ensures easy redispersion (Beck-Broichsitter et al. 2011; El-Naggar et al. 2022a). The Zeta potential distribution in Figure 4A shows a single peak, which is indicative of the high uniformity of CNPs with a

zeta potential value of 27.8 mV, a zeta deviation of 3.75, and coductivity of 0.225 mS/cm at 25 ºC. It also shows reasonable stability among positive-charged CNPs, and this result is consistent with Hussein et al. (2018). Zeta potential distribution of CNPs, which were synthesized utilizing the ionic gelation technique using sodium tripolyphosphate (TPP) as a cross-linking agent, exhibited values ranging from 22.6 to 34.7 mV and had a mean charge of 27 mV (Nasr-Esfahani et al. 2020). Rad et al. (2023) extracted chitosan from the chitin of green shrimp (*Penaeus semisulcatus*) and added a 25% solution of sodium tripolyphosphate for CNP synthesis with a zeta potential value of -19.5 mV. CNPs is positively charged by the NH^{3+} group of the glucosamine units, making it suitable for binding to negatively charged molecules. This positive charge reacts electrostatically with the negatively charged components of biofilms and microbial cell membranes to produce antimicrobial effects (Khan et al. 2020).

X-ray diffraction analysis of CNPs

One popular method of characterizing materials at the nanoscale is X-ray diffraction. XRD is a common characteristic of nanoparticles that is complimentary to other microscopic and spectroscopic approaches, such as phase identification, sample purity, crystallite size, and, in some cases, morphology (Holder & Schaak, 2019). As a result, XRD has been identified as a fingerprint for a specific material. Chitosan always showed two characteristic peaks at 2θ = 10º and 20º as reported by many researchers as El-Naggar et al. (2022c) and Podgorbunskikh et al. (2022). Distinct peaks at 2θ, located at 11.5º, 18.25º, 25.24º, 52.87º, and 72.61º (Figure 4B), were observed in the XRD pattern of the CNPs sample, indicating a shift from the typical chitosan peaks. This shift may be due to the cross-linking between the chitosan and the bioactive compounds presented in the cell-free supernatant of *Paradendryphiella* sp. leading to form a new amorphous polymer of CNPs. the XRD pattern of CNPs is characteristic of an amorphous polymer (Vaezifar et al. 2013). Although the diffraction peak of CNPs and chitosan at 2θ of 11.5º is small, it indicates the hydrated crystalline structure (020) (El-Naggar et al. 2022c; Budi et al. 2020). Additionally, the significant diffraction peak at 2θ = 25.24º was identified in the spectra as reflecting (110) the crystalline structure of anhydrous chitin, indicating the high degree of crystallinity in the chitosan.

Thermal stability of the biosynthesized CNPs

Differential scanning calorimetry (DSC) and thermogravimetric analysis (TGA) were the two primary techniques utilized to determine the thermal stability of the biosynthesized CNPs. DSC is an instrument that is commonly used in thermal analysis to help comprehend the thermal behavior of polymers (Vinodhini et al. 2017; El-Naggar et al. 2022a). Since chitosan is typically a biopolymer, thermal degradation, or the dissociation of its structure, requires a considerable amount of heat energy (Bershtein & Egorov, 1994). Peak enthalpy was shown to be linked with supra-molecular chitin structural compactness (Prashanth et al. 2002). The DSC thermogram of CNPs revealed two separate stages of breakdown, consistent with usual polysaccharide thermal features (El-Naggar et al. 2022c). The DSC curves for CNPs in the current study revealed a significant endothermic peak that was resolved with a T_o value of 79.13 ºC and a T_P value of 119.51 ºC (Figure 5A). The DSC of pure polysaccharide in chitosan curves exhibits endothermic peaks in the 50–150 ºC temperature range, which are linked to the disappearance of volatile components or potential chain relaxation (Fajardo et al. 2010). Feyzioglu & Tornuk (2016) observed that the CNPs showed an exothermic peak at 266 ºC and an endothermic peak at 120.2 ºC, respectively, indicating the disintegration of the CNPs and water evaporation. Furthermore, a broad endothermic peak that was attained below 80 ºC was reported by Vijayalakshmi et al. (2016) as being exceptional for the elimination of absorbed water. According to Coats & Redfern (1963), TGA assesses how a material's chemical and physical characteristics alter while its heating rate changes continuously.

Polymeric nanoparticles are said to be thermally stable if they can resist heat and retain their characteristics at a specific temperature, such as elasticity, toughness, or strength (Charles et al. 2009). A thermogravimetric analyzer (model TGA-50H) was used to assess the thermal characteristics of a sample of 3.8069 mg of biosynthesized CNPs. The sample was treated at 40 mL/min flow rates at temperatures between room temperature and 788.86 ºC (El-Naggar et al. 2022c). The first transition stage of CNPs degradation was initiated by the first weight loss of 0.3513 mg (9.228%) at a temperature of 74.90 ºC (Figure 5B). The second transition stage of CNPs degradation was initiated by the weight loss of 0.4153 mg (10.91%) at a temperature of 197.09 ºC. The first weight loss of CNPs showed the evaporation of ingested water and was detected between 25 and 150 ºC according to Hosseini *et al*. (2013). The third transition stage of is regarded to be the maximum degradation temperature for the CNPs sample, which initiated by the weight loss of 1.562 mg (41.03 %) at a temperature of 368.30 ºC. The final transition stage of CNPs degradation was initiated by the weight loss of 0.8472 mg (22.25%) at a temperature of 788.86 ºC. The weight losses observed in the temperature range of 197.09 to 788.86 ºC may be attributed to the

following processes: the breakdown and decomposition of the polymer chain of the CNPs, chitosan cross-linked with the bioactive component presented in the cell-free supernatant of *Paradendryphiella* sp. and the combustion of the remaining organic components. The increased heat stability is indicative of the hydrogel network becoming stronger and more rigid due to cross-linking (Vijayalakshmi et al. 2016; El-Naggar et al. 2023a). The weight losses observed in the temperature range of 150 to 600 ºC may be ascribed to the following processes: the gradual oxidative degradation of carbonaceous residue; the breakdown and degradation of the polymer chain of the free CS and CS cross-linked with STPP; the disruption of hydrogen bonds between the N-acetyl and free amino groups; and byproducts generated during the previous steps (Mihaela Predescu et al. 2019). CNPs retained a significant percentage of mass, roughly 22.25%, at a heating temperature of 788.86°C despite their reasonable thermal constancy, revealing their high thermal stability.

Time-kill assay and Ultrastructure study of E. dermatitidis upon CNPs treatment

In an attempt to understand the time required by CNPs to kill the examined building-deteriorating fungi (i.e., *E. dermatitidis*) and perceiving their antagonistic dynamics interaction, time kill assay was carried out. Generally, such assay gives a comprehensive insinuation about pharmacodynamics of antimicrobial agents in different detailed manner relative to endpoint assays like minimum inhibitory concentration (MIC). Thus, the main concept of time-kill assay lies behind quantifying the reduction in microbial growth as a function of time and the dose of antimicrobial agent concentration as revealed by Jayathilaka et al. (2022). Initially, the fungal cells were incubated with CNPs at different concentrations (i.e., 50, 125, 250, 500 and 1000 µg/mL) for 120 h; then plated on SDA plates at every 3 h as time interval followed by determining CFU. In the untreated control, all growth phases were noticed, namely, lag, log and stationary phase with viable counts increased by around 0.883 $\log_{10}$ CFU following 24 h incubation time, reached to the maximum at 120 h by 2.141 $\log_{10}$ CFU, respectively, reflecting its slow growth performance comparing to other fungal strains. As depicted in Figure (6), the CNPs showed cell mortality in a time/dose-dependent pattern. Wherein, non-significant reduction in viable count was observed in the treatments of 50 and 125 µg/mL of CNPs by $\log_{10}$ reduction recording 0.58±0.29 (0.076%) and 0.36 ± 0.37 (4.82%), respectively, comparing to the control viable count at 120 h. However, its slow growth rate performance allowed more time for CNPs at doses of 250 and 500 µg/mL to attack the fungal cells causing fungal cytotoxicity, acting thereupon as fungistatic agent up to 30 and 54 h, respectively. That was clearly evident through the drop in CFU/mL values during the initial period of incubation till 24 h. On the other hand, a considerable and significant (*P*–value < 0.0001) decline in the count with fungicidal end point of CNPs was displayed after 33 and 57 h of 250 and 500 µg/mL post-treatment by $\log_{10}$ reduction reached to 4.41 (80.29%) and 3.93 (71.06%), correspondingly (Figure 6A & B). Noteworthy mentioning that the fungicidal or bactericidal potency was accounted for any antimicrobial agent at $\log_{10}$ reduction more than 3 comparing to the original inoculum as referred by Palau et al. (2023). Hereby, the time-course killing curve highlighted that CNPs at concentration of 250 µg/mL shortened the sterilization time required to eradicate the cells of *E. dermatitidis* entirely in 36 h, despite higher concentration (i.e., 500 µg/mL) needed extra time (60 h) to suppress the fungal growth rate and destruct the cells. In addition, Figure (6C) exemplified the relationship between CNPs concentrations and the lethality rate (K value), with R^2 of 0.996. The highest K values were obtained by -0.06 and -0.009 CFU/ml/h with significance recorded (*P*–value < 0.0001) at CNPs concentrations of 250 and 500 µg/mL, correspondingly. Meanwhile, the generation time of *E.dermatitidis* during exponential phase was significantly higher (*P* < 0.05) than its untreated control counterpart (8.02 ± 0.841 h), which recorded 9.93 ± 2.91, 24.9± 3.62 and 11.42 ± 2.91 h for 50, 125 and 1000 µg/mL, respectively. Besides, as depicted in Figure (6D), the kinetic analysis of *E. dermatitidis* indicated the lessening in the fungal growth rate with elevating the concentration of CNPs, which implies that low concentration of CNPs (i.e., 50 and 125 µg/mL) delayed the growth of *E. dermatitidis*, while increasing the concentration up to 500 µg/mL resulted in complete suppression of fungal growth. On the other hand, at 1000 µg/mL the cells of *E. dermatitidis* erratically behaved. Wherein, a progressive decrease in the fungal cells number (CFU/mL) over time was noticed up to 42 h by $\log_{10}$ reduction recorded to 0.556 (10.10%), followed by sudden revival of the survived cells, which accommodated and continued in growth but in slower rate than the control cells. Remarkably, such re-growth phenomenon following exposure to antimicrobial agents could be attributed to the possibility of microbial cells to adapt with environmental stress and generate genetically altered species for better acclimatization to environment changes, in particular with prolonged incubation as referred by Ibrahim et al. (2021). In general, several scholars documented such cell regeneration and resistance phenomenon in several microbial genera as found by (Ibrahim et al. 2021; Vitali et al. 2021; Haitao et al. 2022; Palau et al. 2023).

Strikingly, there was a difference in killing time and growth rate reduction of different microbial genera investigated among frequent published studies. That could be assigned to the overall variations in the cellular physiology, metabolic pattern and their resistance/ susceptibility pattern along with the differences in cell wall architectures and their moieties (Vitali et al. 2021). In general, the chitin is a building block of the fungal cell wall's structure, nonetheless, the association of different entities led to divergence in the interaction's dynamics with CNPs. It is plausible mentioning that *E. dermatitidis*, which is affiliated to black yeast-like fungi family, characterizes by a melanized thick multi-layered cell wall (Kirchhoff et al. 2017) that represents the intrinsic responsibility for distinct tolerance to antifungal agents and extreme environmental conditions (Fonseca et al. 2009).

The SEM micrographs drawn from dark brown pasty and velvety colonies of control or untreated *E. dermatitidis* revealed a compacted and densely backed smooth-walled, elliptical, bottle, cylindrical or flask shaped annellidic conidiogenous cells with size of 1–2 × 1.5–2.6 µm, which were stemmed from the tips and sides of hyphae, aggregated in clusters and arranged tightly in a veil like structure of biofilm extracellular matrix. Such macroconidia secondarily produce blastoconida or budding cells as stated by (Singh et al. 2021). Generally, this dimorphic behavior or polymorphism with evidently switching between yeast and the hyphal phase is significant step in biofilm formation and well-known virulence factor characterizes the cultures of *E. dermatitidis* and contributes mainly in its pathogenicity (Kirchhoff et al. 2017; Kirchhoff et al. 2020). However, pseudohyphae (red arrow), true septate hyphae (white arrows), and sclerotic bodies (green arrows) were also detected along with budding yeast cells. Additionally, the annellations or truncated scars were also observed in some cells (navy blue arrows). Remarkably, all theses characterstic fungal traits are numerously documented by several studies (Liu et al. 2004; Woo et al. 2013; Kirchhoff et al. 2019; Yoshinouchi et al. 2023).

Intriguingly, upon CNPs treatment, certain dramatic morphological alterations were noticed. The macroconidia or budding cells showed swelling, enlarged size more than normal cells, crinkling of cells and mycelia surfaces (Red dashed arrows). Besides, CNPs deteriorated the biofilm architecture reflected from the lowering the number of cells in the biofilm biomass and lessening biofilm density as deduced from the absence of exopolysaccharide matrix that encompasses the cells. In addition, lumpy appearance with numerous wide holes and indentations decorated the surface of yeast cells was clearly observed (dashed green arrows), revealing lethal deformation of cell's membranes, infiltration of intracellular cytoplasmic constituents and ultimately cell death. Let alone the absence of pseudo-hyphae, sclerotic bodies and lacking of condense hyphae clumping, which imply the losing of cells pathogenicity. Notably, all such cellular damage symptoms characterize the cells of *E. dermatitidis* upon exposure to various antifungal medications (Kirchhoff et al. 2020; Liu et al. 2004).

Apparently, the antimycotic performance of CNPs could be attributed to their nanoscale dimensions of chitosan with polycationic nature. As an initial step, an enhanced electrostatic attraction and strong binding potency suggested to be implemented between the highly abundant amino groups (NH^{3+}) in N-acetylglucosamine units of chitosan structure and the negatively charged functional groups disseminates on *E. dermatitidis* cell membranes (El-Naggar *et al*. 2023a)**.** Followed by augmented penetration capability of chitosan molecule and capturing of essential metals from surrounding circumference by the dint of higher surface area of tiny particles with metal-chelating property. All such characterstic features aid intensively in frustrating the incorporation of metal ions in their corresponding functional sites of fungal biomolecules membranes (El-Naggar *et al*. 2023b). Moreover, the glucopyranoside rings of chitosan symbolizes by their hydrophobicity, which participates substantially in inserting or translocating into the hydrophobic tail part of lipid, by such way implementing membranolytic activity. Strikingly, such membranolytic trait could be deduced from SEM micrographs, in the current study. Wherein, the morphological changes with wide furrows on the surfaces of the wrinkled cell implied the disruption of cell membrane integrity, inducing osmotic imbalances, elevating wall permeability, which increase the intracellular leakage rate and thwart the development of extracellular polymeric matrix; utterly destabilize the biofilm formation and impede viability and pathogenicity of *E. dermatitidis* cells. Remarkably, the antimicrobial property of CNPs due to membranolytic action was documented by previous studies (Park et al. 2015). Nonetheless, the fungistatic activity of CNPs was found by some studies rather than fungicidal activity (Rabea et al. 2003; Goy et al. 2009). Such different results found by various scholars could be assigned to variations in the overall CNPs physicochemical properties (e.g., shape, dimensions, agglomeration, surface charge, etc.), which are tightly relevant to synthesis protocols, types of reducing agents and also capping agents. While the microbial performance, metabolic activity, kinds and the treated count simultaneously with different exposure time, different pH and temperature are also decisive parameters (El-Naggar *et al*. 2023b).

Conclusively, the natural origin, biocompatibility and considerable safety in addition to the outstanding fungicidal potentiality of our mycosynthesized CNPs, in dampening fungal growth and necrotizing the switching between biofilm architecture and hyphal phase of *E. dermatitidis*, encourage their application as hygienic coat or conserving paint against building biodeteriorator microbes. However, their eco-friendliness enables restorers and conservators to safely utilize CNPs in self-protection and mycological resistance for preserving buildings, in particular museums, cultural heritage, archives, food processing/ storage/ packaging industry and hospitals in lieu of banned synthetic paints.

Conclusions

To sum up, the current study introduces a novel approach of CNPs biosynthesis using the cell-free supernatant of *Paradendryphiella* sp. To the best of our knowledge, no previous studies have reported the synthesis of CNPs by *Paradendryphiella* sp. The cell-free supernatant of *Paradendryphiella* sp. has been proved as effective crosslinking and stabilizing agent by several characterization experiments. Fascinatingly, this study also demonstrated the promising fungicidal potency of the myco-synthesized CNPs against the fungus *Exophiala dermatitidis* as a model of meristematic black fungi that causes building biodeterioration. So, it is recommended to employ CNPs as an anti-bioreceptivity painting material for building preservation.

List of abbreviations

Chitosan nanoparticles	CNPs
Scanning electron microscope	SEM
Transmission electron microscope	TEM
Fourier transform infrared	FTIR
Energy-dispersive X-ray spectroscopy	EDX
X-ray diffraction	XRD
Differential scanning calorimetry	DSC
Thermogravimetric analysis	TGA
Extracellular polymeric matrix	(EPS
Tripolyphosphate	TPP
Sabouraud dextrose agar	SDA
Melting temperature	T_m
Glass transition	T_g
Sabouraud dextrose agar	SDA
Colony forming unit	CFU
Minimum inhibitory concentration	MIC

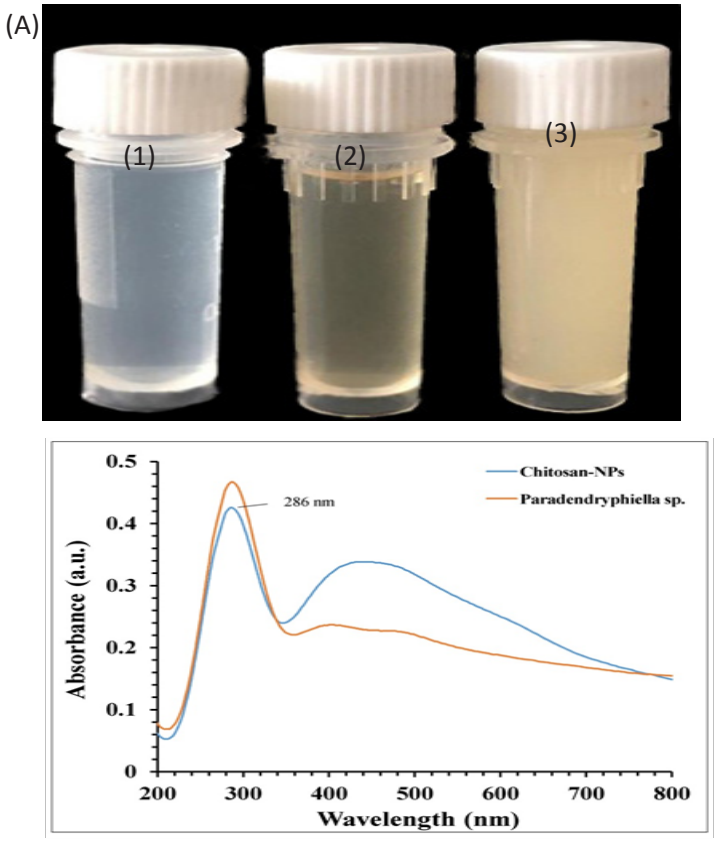

Fig.1 A) Vials of chitosan solution (1), cell-free supernatant of *Paradendryphiella* sp (2), chitosan-NPs (3), B) UV-Vis absorbance of the chitosan-NPs and the cell-free supernatant of *Paradendryphiella* sp.

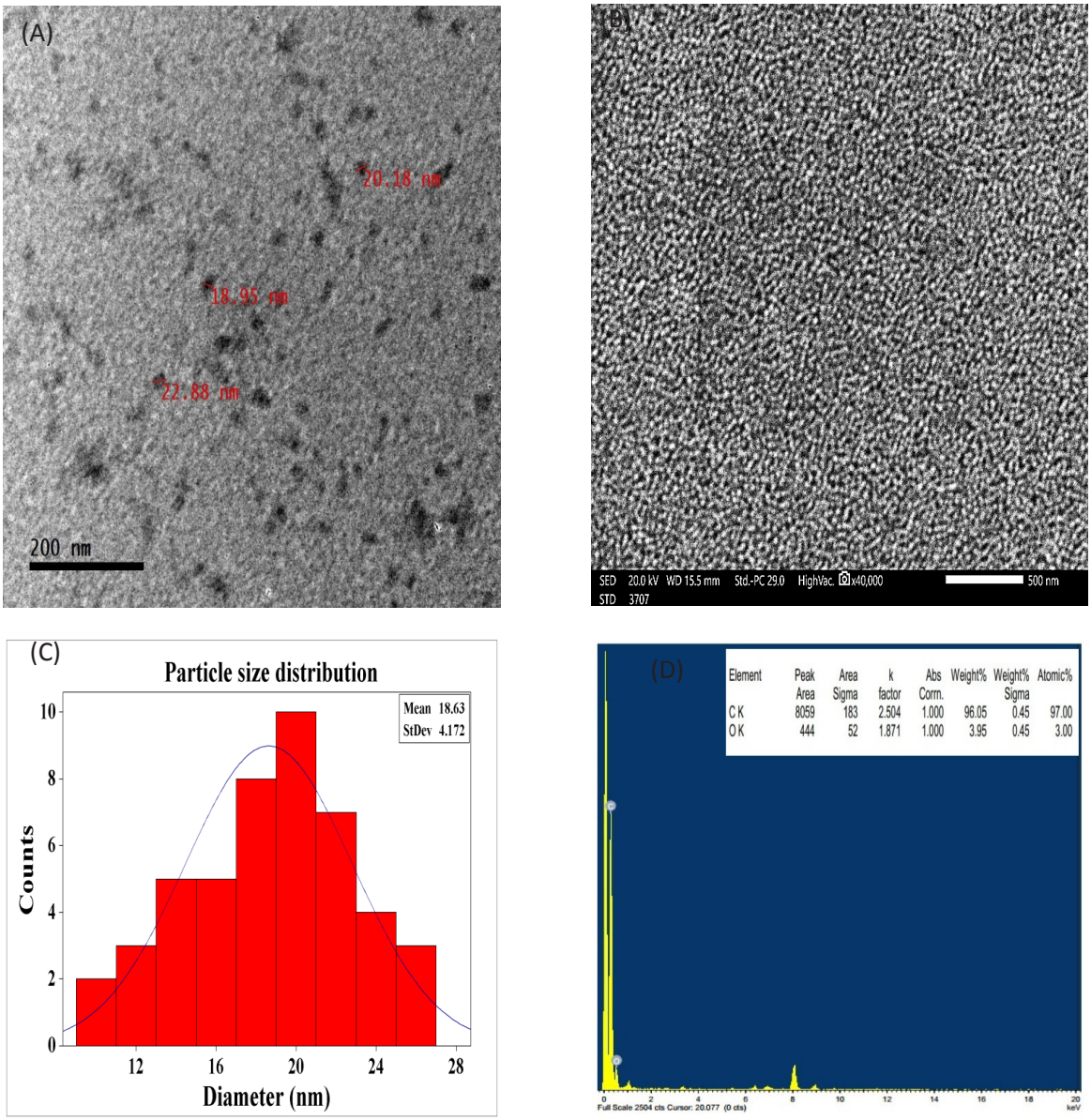

Fig.2. TEM analysis of CNPs (A), SEM analysis of CNPs (B), particle size analysis of CNPs (C), EDX analysis (D).

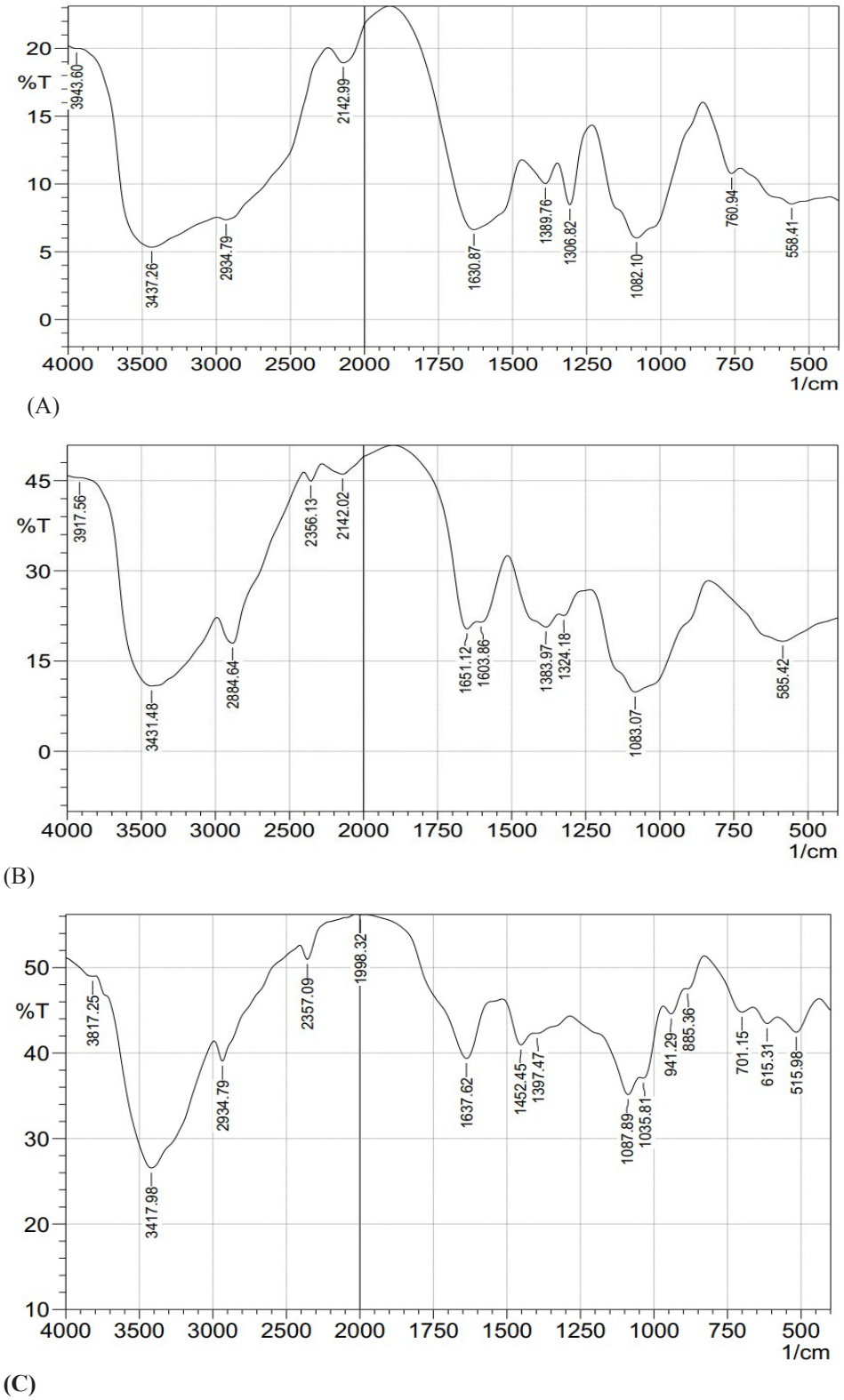

Fig.3. FTIR of the biosynthesized CNPs (A), chitosan standard (B), and the cell-free supernatant of *Paradendryphiella* **sp. (C).**

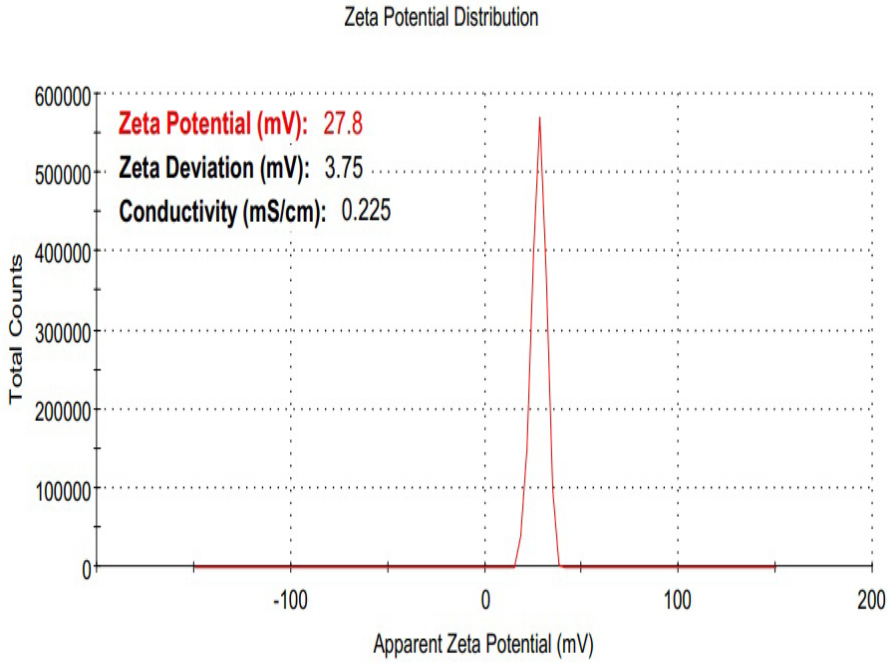

(A)

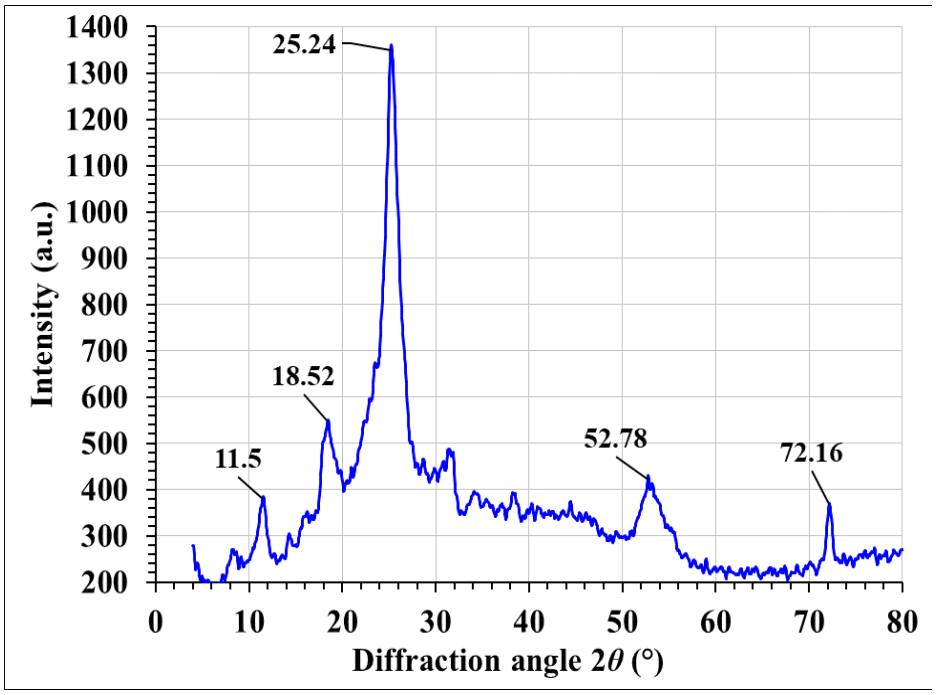

(B)

Fig.4 . (A) Zeta potential and (B) XRD of the biosynthesized CNPs.

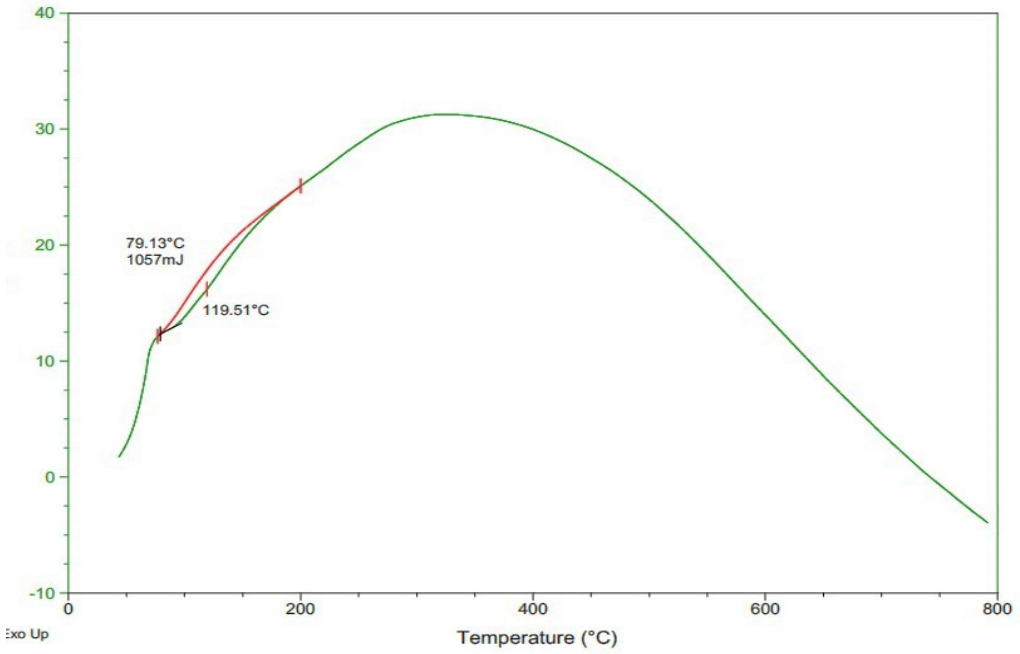

(A)

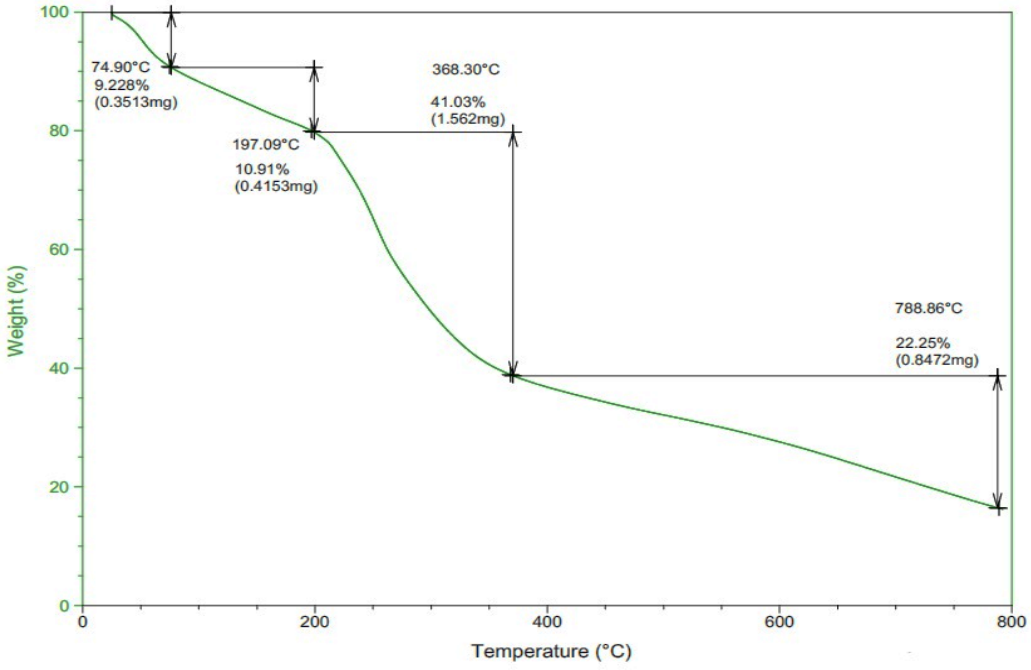

(B)

Fig. 5 . DSC (A) and TGA (B) analyses of CNPs.

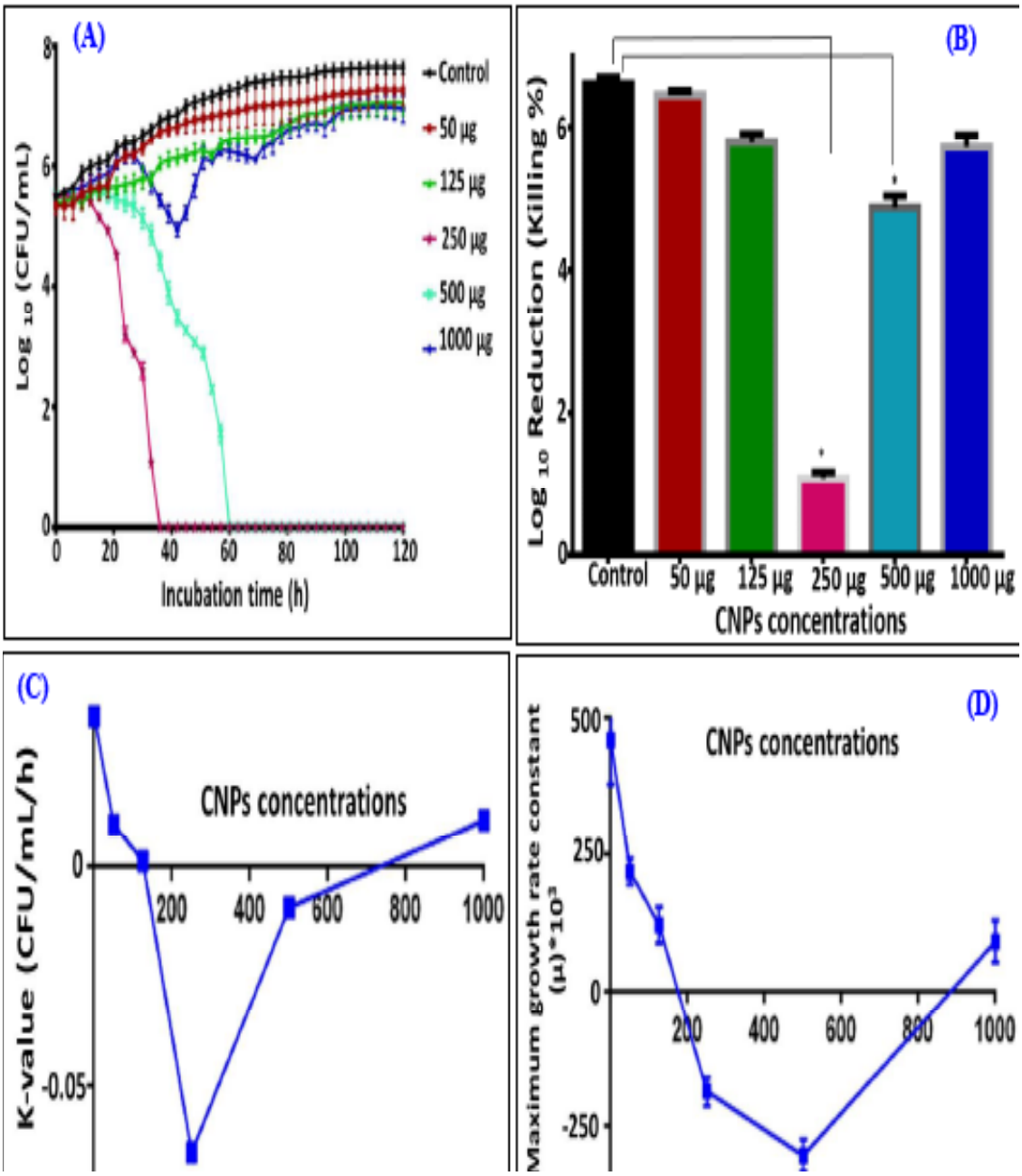

Fig. 6 The effect of CNPs on fungal growth of *E. dermatitidis* (A)-Typical pattern of kill curves on *Exophiala dermatitidis* at different concentrations of CNPs (µg/mL) as a function of treatment time (h), (B) log10 reduction and killing percentage of each examined concentration, (C)-The relationship between K-value and each examined concentration revealing lethality and (D)-The relationship between growth rate and different CNPs concentrations .

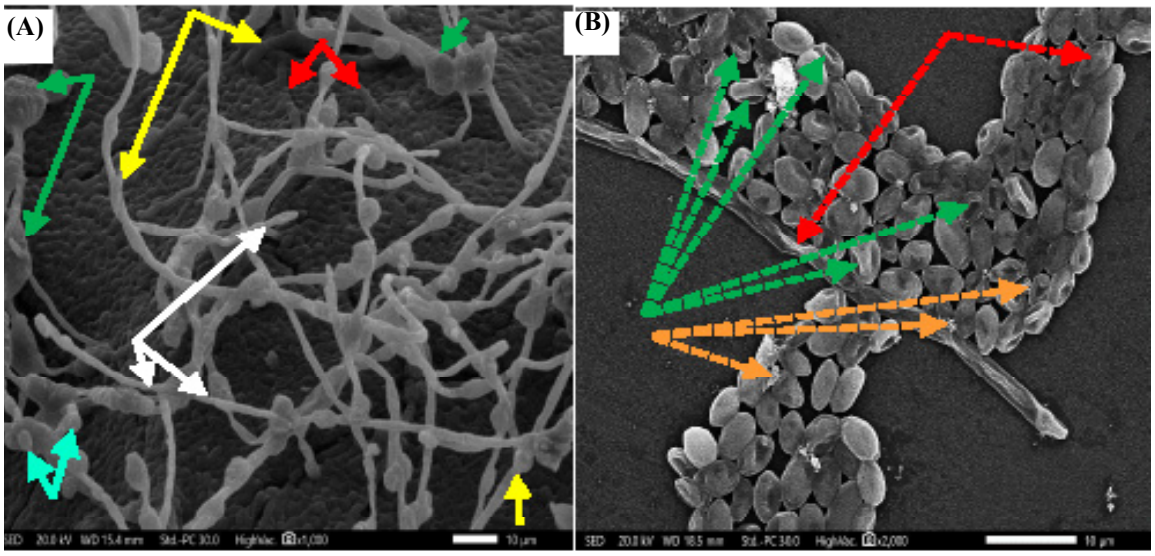

Fig.7. SEM micrographs of *E. dermatitidis* depicting the morphological changes induced by mycosynthesized CNPs. A) - Control untreated cells, B) - CNPs-treated cells. Red arrows: pseudohyphae, White arrows: true septate hyphae, Green arrows: sclerotic bodies, Green arrows: septa of true hyphae, Yellow arrows: flask-shaped to cylindrical annellides conidiogenous yeast cells forming biofilm, Navy blue arrows: annellated budding yeast cells with truncated scars, Red dashed arrows: deformed hyphae with crinkling surfaces, Dashed green arrows: holes and indentations and Dashed orange arrows: CNPs.

Declarations

Ethics approval and consent to participate

This investigation has not involved any human subjects or animal participants.

Adherence to national and international regulations

Not applicable.

Consent for publication

Not applicable.

Availability of data

https://www.ncbi.nlm.nih.gov/search/all/?term=OQ134928

Competing interests

The authors declare that they have no competing interests.

Funding

No funding

Authors' contributions

H.E. conducted the experiments, provided the fungal isolate, contributed to the writing and revision of the manuscript. N.E.E. proposed the research topic, designed the research plan, provided necessary tools for the experiments and experimental instructions, conducted instrumentation analyses, contributed to the writing, rephrasing and critically revised the manuscript. A.A.E. contributed to the writing, analyzing, discussing the instrumentation results, revision of the manuscript and preparation of the manuscript for Journal submission. M.E. designed the research plan, provided necessary tools for the experiments contributed to the writing of the manuscript, rephrasing and critically revised the manuscript. All authors read and approved the final manuscript.

Acknowledgements

The authors gratefully acknowledge the City of Scientific Research and Technological Applications (SRTA-City), Alexandria, 21934, Egypt, for providing financial support for most laboratory measurements and analyzes of this paper within the framework of SRTA-City Central Laboratories Services**.**

References

Aldosari M A, *et al* (2019) Using ZnO nanoparticles in fungal inhibition and self-protection of exposed marble columns in historic sites. Arc ant sci 11: 3407-22.

Banach M, *et a*l (2014) Building materials with antifungal efficacy enriched with silver nanoparticles. Chem Sci J 5: 085.

Beck-Broichsitter M, et *al* (2011) Biophysical investigation of pulmonary surfactant surface properties upon contact with polymeric nanoparticles *in vitro*. Nanomed nanotech **7:** 341350.

Bekmukhametova A, *et al* (2022) Fabrication and characterization of chitosan nanoparticles using the coffee-ring effect for photodynamic therapy. LSM 54:758–766.

Bershtein V A, Egorov V M (1994) Differential scanning calorimetry of polymers: physics, chemistry, analysis, technology, Ellis Horwood, New York, London, Toronto, Sydney, Singapore.

Berti L, Marvasi M, Perito B (2023) Characterization of the Community of black meristematic fungi inhabiting the external white marble of the florence cathedral. J Fungi (Basel) 9(6): 665.

Binesh N, Farhadian N, Mohammadzadeh A (2021) Enhanced stability of salt-assisted sodium ceftriaxone-loaded chitosan nanoparticles: Formulation and optimization by 32-full factorial design and antibacterial effect study against aerobic and anaerobic bacteria. Colloids Surf. A: Physicochem Eng Asp 618: 126429.

Bodnar M, Hartmann J F, Borbely J (2005) Preparation and characterization of chitosan-based nanoparticles. Biomacromol 6(5): 2521–2527.

Budi S, Suliasih B A, Rahmawati I (2020) Size-controlled chitosan nanoparticles prepared using ionotropic gelation. Sci Asia 46(4): 457–461.

Çakır M A, Icyer N C, Tornuk F (2020) Optimization of production parameters for fabrication of thymol-loaded chitosan nanoparticles. Int J Biol Macromol 151: 230–238.

Cantón E, *et al* (2004) Patterns of amphotericin B killing kinetics against seven Candida species. AAC 48(7):2477-82.

Charles J, *et al* (2009) FTIR and thermal studies on nylon-66 and 30% glass fibre reinforced nylon-66. E J Chem 6: 23–33.

Coats A W, Redfern J P (1963) Thermogravimetric analysis. A review. Analyst 88(1053): 906–924.

Duraisamy N *et al* (2022) Green synthesis of chitosan nanoparticles using of *Martynia annua* L. ethanol leaf extract and their antibacterial activity. Crystals 12(11):1550.

El-Naggar N E A, *et al* (2022a) An innovative green synthesis approach of chitosan nanoparticles and their inhibitory activity against phytopathogenic *Botrytis cinerea* on strawberry leaves. Sci Rep 12(1): 3515.

El-Naggar N E A (2022b) Innovative biosynthesis, artificial intelligence-based optimization, and characterization of chitosan nanoparticles by *Streptomyces microflavus* and their inhibitory potential against *Pectobacterium carotovorum*. Sci Rep 12(1):21851.

El-Naggar NEA, *etal* (2022c) Green synthesis of chitosan nanoparticles, optimization, characterization and antibacterial efficacy against multi drug resistant biofilm-forming *Acinetobacter baumannii*. Sci Rep 12: 19869.

El-Naggar N E A, et *al* (2023a) Green fabrication of chitosan nanoparticles using *Lavendula angustifolia*, optimization, characterization and in-vitro antibiofilm activity. *Sci Rep* 13: 11127.

El-Naggar N E A, *et al* (2023b) Artificial intelligence-based optimization for chitosan nanoparticles biosynthesis, characterization and in-vitro assessment of its anti-biofilm potentiality. Sci Rep 13: 4401.

El-Naggar N E A, *et al* (2024) A sustainable green-approach for biofabrication of chitosan nanoparticles, optimization, characterization, its antifungal activity against phytopathogenic *Fusarium culmorum* and antitumor activity. Sci Rep 14(1): 11336.

El-Sawah A A, et *al* (2024a) Green synthesis of collagen nanoparticles by *Streptomyces xinghaiensis* NEAA-1, statistical optimization, characterization, and evaluation of their anticancer potential. Sci Rep 14: 3283.

El-Sawah A A, et *al* (2024b) Bionanofactory for green synthesis of collagen nanoparticles, characterization, optimization, in-vitro and in-vivo anticancer activities. Sci Rep 14: 6328

El-Shall H, Abu-Serie M, Abu-Elreesh G, Eltarahony M (2023) Unveiling the anticancer potentiality of single cell oils produced by marine oleaginous *Paradendryphiella sp.* under optimized economic growth conditions. Scienti Repor. 26:20773.

Fajardo A R, et al (2010) Time-and pH-dependent self-rearrangement of a swollen polymer network based on polyelectrolytes complexes of chitosan/chondroitin sulfate. Carbohydr Polym 80(3): 934-943.

Feyzioglu G C, Tornuk F (2016) Development of chitosan nanoparticles loaded with summer savory (*Satureja hortensis* L.) essential oil for antimicrobial and antioxidant delivery applications. Lebensmittel-Wissenschaft Technol 70: 104-110.

Fonseca F L, *et al* (2009) Structural and functional properties of the *Trichosporon asahii glucuronoxylomannan*. Fungal Genet Biol 46(6-7): 496-505.

Ganguli P, Chaudhuri S (2021). Nanomaterials in antimicrobial paints and coatings to prevent biodegradation of man-made surfaces: A review. Mater Today: Proceedings 45: 3769-77.

Goy R C, Britto D, Assis O B G (2009) A review of the antimicrobial activity of chitosan. Polímeros: Ciênc Tecnol 19: 241–247.

Gutarowska B, *et al* (2012) Analysis of the sensitivity of microorganisms contaminating museums and archives to silver nanoparticles. Biodegradation 68: 7-17.

Ha N M C, *et al* (2019) Preparation of NPK nanofertilizer based on chitosan nanoparticles and its effect on biophysical characteristics and growth of coffee in green house. Rev Chem Intermed 45(1): 51–63.

Haitao Y, *et al* (2022) A novel polymeric nanohybrid antimicrobial engineered by antimicrobial peptide MccJ25 and chitosan nanoparticles exerts strong antibacterial and anti-inflammatory activities. Front Immunol 12: 811381.

Haris P I, Severcan F (1999) FTIR spectroscopic characterization of protein structure in aqueous and non-aqueous media. J Mol Catal B-Enzym **7**: 207–221.

Holder C F, Schaak R E (2019) Tutorial on powder X-ray diffraction for characterizing nanoscale materials. Acs Nano 13**(**7): 7359-7365.

Hosseini S F, *et al* (2013). Two-step method for encapsulation of oregano essential oil in chitosan nanoparticles: Preparation, characterization and in vitro release study. *Carbohydr Polym 95*: 50–56.

Huanbutta K, *et al* (2023) Key fabrications of chitosan nanoparticles for effective drug delivery using flow chemistry reactors. Int J Nanomedicine 7889-7900.

Hussein A, *et al* (2018) Improvement of 6 mercaptopurine efficiency by encapsulated in chitosan nanoparticles. AJNSA 51: 181-186.

Ibrahim A, Moodley D, Uche C (2021) Antimicrobial and cytotoxic activity of electrosprayed chitosan nanoparticles against endodontic pathogens and Balb/c 3T3 fibroblast cells. Sci Rep 11: 24487.

Jayathilaka E T, *et a*l (2022) Antimicrobial peptide octominin-encapsulated chitosan nanoparticles enhanced antifungal and antibacterial activities. Int J Mol Sci 23(24): 15882.

Joseph E (2021) Microorganisms in the Deterioration and Preservation of Cultural Heritage. Springer Nature

Khan F, et *al* (2020) Chitosan and their derivatives: Antibiofilm drugs against pathogenic bacteria. Colloids Surf Biointers 185, 110627.

Khanmohammadi M, Elmizadeh H, Ghasemi K (2015) Investigation of size and morphology of chitosan nanoparticles used in drug delivery system employing chemometric technique. Iran J Pharmaceut Res *(IJPR)* 14(3): 665.

Khare T, *et al* (2021) Embelin-loaded chitosan gold nanoparticles interact synergistically with ciprofloxacin by inhibiting efflux pumps in multidrug-resistant *Pseudomonas aeruginosa* and *Escherichia coli*. Environ Res 199: 111321.

Kim Y H, *et al* (2020) Comparative antibacterial and antifungal activities of sulfur nanoparticles capped with chitosan. Microb Pathog 144: 104178.

Kim Y H, *et al* (2022) Synthesis of fully deacetylated quaternized chitosan with enhanced antimicrobial activity and low cytotoxicity. Antibiotic 11(11):1644.

Kirchhoff L (2020) Phenotypical characteristics of the black yeast *Exophiala dermatitidis* are affected by *Pseudomonas aeruginosa* in an artificial sputum medium mimicking cystic fibrosis–like conditions. Front Microbial 11: 471.

Kirchhoff L, *et al* (2017) Biofilm formation of the black yeast-like fungus *Exophiala dermatitidis* and its susceptibility to antiinfective agents. Sci Rep 7(1): 42886

Kirchhoff L, *et al* (2019) Exophiala dermatitidis: key issues of an opportunistic fungal pathogen. Virulence 10 (1): 984-98.

Lambert J B (1987) Introduction to Organic Spectroscopy. Macmillan.

Liu H, *et al* (2004) Wangiella (Exophiala) dermatitidis WdChs5p, a class V chitin synthase, is essential for sustained cell growth at temperature of infection. Eukaryotic Cell 3(1): 40-51.

Liu X, et *al* (2020) Microbial deterioration and sustainable conservation of stone monuments and buildings. Nat Sustain 3(12): 991-1004.

Makhlof A, Tozuka Y, Takeuchi H (2011) Design and evaluation of novel pH-sensitive chitosan nanoparticles for oral insulin delivery. Eur J Res 42(5): 445-451.

Mihaela Predescu A, *et a*l (2019) Adsorption of lead (II) from aqueous solution using chitosan and polyvinyl alcohol blends. Anal Lett 52, 2365–2392.

Mukhopadhyay P, *et al* (2013) Oral insulin delivery by self-assembled chitosan nanoparticles: *in vitro* and *in vivo* studies in diabetic animal model. Mater sci eng 33(1): 376–382.

Nasr-Esfahani M, Doosti A, Sazegar H (2020) Evaluation of the immune response against *Helicobacter pylori* in infused BALB/c mice by pcDNA3. 1 (+)-ureA. Folia Medica 62(1).

Nasti A, *et al* (2009) Chitosan/TPP and chitosan/TPP-hyaluronic acid nanoparticles: systematic optimization of the preparative process and preliminary biological evaluation. Pharm Res 26(8): 1918-1930.

Ngene A, *et al* (2024) Time-kill kinetics and antibacterial activity of ethanolic extract of *Allium sativum*. Microbes Infect 5(1): 389-97.

Nguyen T V, *et al* (2017) Preparation of chitosan nanoparticles by TPP ionic gelation combined with spray drying, and the antibacterial activity of chitosan nanoparticles and a chitosan nanoparticle–amoxicillin complex. Rev Chem Intermed 43(6): 3527–3537.

Palau M, *et al* (2023) In vitro antibacterial activity of silver nanoparticles conjugated with amikacin and combined with hyperthermia against drug-resistant and biofilm-producing strains. Microbiol Spectr 11(3): 00280-23.

Park S C, *et al* (2015) Antimicrobial action of water-soluble β-chitosan against clinical multi-drug resistant bacteria. Int J Mol Sci 16(4): 7995-8007.

Pinna D (2021) Microbial growth and its effects on inorganic heritage materials. . In: Joseph, E. (eds) Microorganisms in the Deterioration and Preservation of Cultural Heritage. Springer, Cham.

Podgorbunskikh E, *et al* (2022). Mechanical amorphization of chitosan with different molecular weights. Polymers 14 (20): 4438.

Prashanth K H, Kittur F S, Tharanathan R N (2002) Solid state structure of chitosan prepared under different N-deacetylating conditions. Carbohydr Polym 50(1): 27-33.

Rabea E I, *et al* (2003) Chitosan as antimicrobial agent: applications and mode of action. Biomacromol 4(6): 1457-65.

Rad S K, et *al* (2023) Effect of Chitosan Nanoparticle on pfLA and ftsL Genes Expression in Listeria monocytogenes. Int J Infect 10(1).

Raj L A, *et al* (2015) Preparation and characterization of BSA and chitosan nanopartices for sustainable delivery system for quercetin. J Appl Pharm Sci 5(7): 001-005.

Raja P B (2022) Characterization of nanomaterial used in nanobioremediation. In Nano-bioremediation: fundamentals and applications. Elsevier, 57-83.

Rasaee I, Ghannadnia M, Honari H (2016) Antibacterial properties of biologically formed chitosan nanoparticles using aqueous leaf extract of *Ocimum basilicum*. Nanomed J 3(4): 240–247.

Sathiyabama M, *et al* (2024) Green synthesis of chitosan nanoparticles using tea extract and its antimicrobial activity against economically important phytopathogens of rice. Sci Rep 14(1): 7381.

Scheerer S, Ortega-Morales O, Gaylarde C (2009) Microbial deterioration of stone monuments—an updated overview. Adv Appl Microbiol 66: 97-139.

Sharifi-Rad J, *et a*l (2021) Chitosan nanoparticles as a promising tool in nanomedicine with particular emphasis on oncological treatment. Cancer Cell Int 21(1): 1-21.

Sierra-Fernández A, *et al* (2017) New nanomaterials for applications in conservation and restoration of stony materials: A review, Mater de construcción 67: 325.

Singh S, *et al* (2021) Clinical spectrum, molecular characterization, antifungal susceptibility testing of *Exophiala* spp. from India and description of a novel *Exophiala* species, *E. arunalokei* sp. nov. Front cell infect microbiol 11: 686120.

Subramanian A, Abraham G, Honnavar P (2022) *Trichosporon asahii* infection associated with glomerulonephritis in a diabetic patient. Med Mycol Case Rep 35: 15-7.

Vaezifar S, *et al* (2013) Effects of some parameters on particle size distribution of Chitosan nanoparticles prepared by ionic gelation method. J clust sci 24 (3), 891–903.

Van S N, Minh H D, Anh D N (2013) Study on chitosan nanoparticles on biophysical characteristics and growth of Robusta coffee in green house. Biocatal Agric Biotechnol. 2: 289–294.

Vijayalakshmi K, *et al* (2016) Synthesis, characterization and applications of nanochitosan/ sodium alginate/microcrystalline cellulose film. J Nanomed. Nanotechnol **7**(419): 2.

Vinodhini P A, et al (2017) FTIR, XRD and DSC studies of nanochitosan, cellulose acetate and polyethylene glycol blend ultrafiltration membranes. Int J Biol Macromol 104: 1721–1729.

Vitali A, *et al* (2021) Antifungal carvacrol loaded chitosan nanoparticles. Antibiotic 11(1): 11.

Wardani G, et al (2022) Antioxidative stress and antiapoptosis effect of chitosan nanoparticles to protect cardiac cell damage on streptozotocin-induced diabetic rat. Oxid Med Cell Longev .

Wardani G, Sudjarwo S A (2018) In vitro antibacterial activity of chitosan nanoparticles against Mycobacterium tuberculosis. Pharmacogn *J* 10(1): 162–166.

Woo P C *et al* (2003) Clinical spectrum of Exophiala infections and a novel Exophiala species, *Exophiala hongkongensis*. J Clin Microbiol 51(1): 260-7.

Xing Y, *et al* (2021) Comparison of antimicrobial activity of chitosan nanoparticles against bacteria and fungi. Coatings 11(7): 769.

Yanat M, Schroën K (2021) Preparation methods and applications of chitosan nanoparticles; with an outlook toward reinforcement of biodegradable packaging. React Func Pol 161, 104849.

Yoshinouchi T, *et al* (2023) Diagnosis and clinical management of *Exophiala dermatitidis* pneumonia in a patient with anorexia nervosa: A case report. Med Mycol Case Rep 42: 100617.

Zhang HL, *et al* (2010) Preparation and characterization of water-soluble chitosan nanoparticles as protein delivery system. J. Nanomater 1-5.